Mist CVD of Vanadium Dioxide Thin Films with Excellent Thermochromic Properties Using a Water-Based Precursor Solution

Yuya Matamura, Takumi Ikenoue, Masao Miyake* and Tetsuji Hirato

Graduate School of Energy Science, Kyoto University, Yoshida-honmachi, Sakyo-ku, Kyoto 606-8501, Japan

Email: miyake.masao.4e@kyoto-u.ac.jp

Abstract

Mist chemical vapor deposition (mist CVD), which is capable of producing oxide films over large areas at a high productivity and low cost, has been proposed as a fabrication method for VO_2 thin films for smart windows. However, the thermochromic properties of the VO_2 films previously prepared by mist CVD are not sufficient for application in smart windows. In this study, to obtain a high-quality VO_2 film, we investigated the effects of the solvent of the precursor solution on the resulting film in mist CVD. Films consisting of a single phase of VO_2 were obtained when a water-based precursor solution was used. In contrast, V_2O_3 films are formed when a methanol-based precursor solution is used. The VO_2 film deposited from water solution exhibited high visible transmittance along with a large change in the infrared transmittance with temperature change. The high quality of the VO_2 film indicates that mist CVD is an effective method for the fabrication of VO_2-based smart windows.

Keywords: Vanadium dioxide, Chemical vapor deposition, Smart window, Thermochromic window, Mist CVD.

1. Introduction

Transition-metal oxides exhibit interesting electrical, optical and magnetic properties, which have attracted considerable attention as promising materials for devices used in energy fields, such as solar cell [1–5], batteries [6,7], sensors [8] and smart windows [9,10]. One of the most fascinating devices is the smart window that utilizes metal-insulator transition (MIT) of vanadium dioxide (VO_2). MIT of VO_2 occurs at about room temperature [11–18]. Both visible and infrared lights are transmitted through VO_2 below the phase transition temperature (T_c); however, above T_c, only visible light is transmitted [19,20]. Owing to this property of VO_2, the windows coated with VO_2 block infrared light from entering when it is hot outside, while still allowing the transmission of visible light. Infrared radiation, which accounts for approximately 50% of the solar radiation energy, is the heat source that flows in buildings. Therefore, the control of the heat intake through VO_2-based smart windows can effectively reduce the amount of energy consumed for air conditioning in a building.

VO_2 thin films can be fabricated by various methods such as the hydrothermal method [14,21,22], sol–gel method [23], pulsed laser deposition [24], sputtering [25,26], atomic layer deposition [27] and chemical vapor deposition (CVD) [28,29]. However, physical vapor deposition and conventional CVD require vacuum equipment, resulting in high process costs. Solution processes generally require a long reaction time of more than several hours for the fabrication of a VO_2 thin film, thus resulting in low productivity [14,21,22]. For practical mass production of VO_2-based smart windows for buildings, a low-cost and highly productive fabrication process for VO_2 should be developed.

As a low-cost and highly productive deposition process, mist CVD, which is also referred to as aerosol-assisted CVD, has been proposed in previous studies [30–36]. In mist CVD, a mist of precursor solution atomized by ultrasonic vibrations is supplied to the substrate with a carrier gas, and thermal decomposition of this precursor mist results in a film formation on the substrate. Since no vacuum system is required in this process, highly productive and low-cost films can be produced. However, to date, no VO_2 thin films with sufficient performance have been obtained through mist CVD. The visible transmittance reported for VO_2 films fabricated through mist CVD is generally <40% at a wavelength of 550 nm, and the change in the infrared transmittance at a wavelength of 2500 nm below and above *T*c is also as small as <30 percentage point (pp) [37–42]. For other oxide films, such as Ga_2O_3 and ZnO, high-quality films comparable to those obtained by vacuum processes are produced through mist CVD [31,36]. Therefore, it is expected that high-quality VO_2 films can also be obtained through mist CVD by exploring

the deposition conditions in further detail.

The optical properties of VO_2 are strongly affected by its stoichiometry. Contaminating a VO_2 crystal with V^{3+} and V^{5+} deteriorates its visible transmittance and infrared transmittance change [43–45]. Although films composed of a VO_2 single phase were reportedly obtained through mist CVD using an ethanol solution of vanadyl acetylacetonate ($VO(acac)_2$) as the precursor [39], further control of the stoichiometry of the VO_2 film is necessary to enhance its properties.

In mist CVD, metal salt and the solvent of the precursor solution are the factors that can significantly affect the crystal phase and physical properties of the resulting film, because the latter can change the oxygen potential of the deposition atmosphere [39,46,47]. A study on the oxidation of V_2O_3 to VO_2 reported that a water vapor atmosphere is suitable for stabilizing vanadium in the tetravalent state [48,49]. Although it was reported that mist CVD using a precursor solution composed of vanadium(III) acetylacetonate ($V(acac)_3$) and water resulted in V_2O_3 [39], mist CVD using a combination of tetravalent vanadium salt and water has not yet been investigated.

In this study, we perform mist CVD of vanadium oxide using a methanol solution and a water solution of $VO(acac)_2$ to investigate the effect of the solvent on the crystal phase of the resulting film. Furthermore, we demonstrate that VO_2 films with high visible transmittance and a large infrared transmittance change by MIT are obtained through mist CVD using a water-based precursor solution.

2. Experimental

2.1. Materials

The precursor solutions were prepared by dissolving bis(acetylacetonato) vanadium oxide ($VO(acac)_2$; 98%, STREM) in distilled water or methanol at a concentration of 0.010 mol/L. A quartz plate (25 mm × 25 mm; thickness = 0.7 mm) was used as the substrate for mist CVD. Before use, the quartz substrate was washed sequentially in acetone, distilled water and isopropanol in an ultrasonic cleaner and dried by blowing air.

2.2. Mist CVD of VO_2

A custom-built hot-wall mist CVD system (Fig. 1) was used for the deposition of the VO_2 films. The apparatus and deposition procedure of mist CVD in this study were

the same as those described in our previous report [40], except for the method of placing the substrate. Herein, the substrate was placed on a holder installed at the center of the tube furnace. The precursor mist was supplied to the substrate through N_2 flow for 10 min and 20 min in the cases of using a methanol solution and water solution, respectively, as the precursor. The durations for the film growth were determined by considering the difference in the amount of mist generated from two different solvents. The flow rate of the carrier gas and dilution gas was 3.0 L min^{-1}. After the mist supply was turned off, the substrate was cooled to <100 °C in a furnace under N_2 gas flow.

2.3. Characterization of films

X-ray diffraction (XRD) measurements were performed with an X-ray diffractometer (X'pertPRO-MPD, PANalytical) using Cu Kα radiation to identify the crystal phases of the obtained films. The incident angle was fixed at ω = 1.5°. The morphology of the films was observed through field emission scanning electron microscopy (SEM, JSM-6510LV, JEOL) and atomic force microscopy (AFM, Nano Navi IIs Nanocute, SII Nano Technology). The cross-section of the film was observed after Au sputtering using a sputter coater (SC-701, SANYUELECTRON). X-ray photoelectron spectroscopy (XPS) was performed using a JPS-9030 spectrometer (JEOL) to analyze the chemical states of the elements present in the obtained films. The details of the XPS measurements are described in the Supplementary material. The electrical resistivity was measured by a four-probe method using a source meter (2450 SourceMeter, KEITHLEY) while changing the temperature of the films using a hot plate. The temperature of the film was measured using a thermocouple attached to the film. The logarithmic derivatives of the temperature dependence of resistivity (d(log$R$)/dT) were extracted to evaluate the phase transition temperature (T_c) and width of the hysteresis loop (ΔH). Further, T_c and ΔH were defined using the temperature corresponding to the maximum of d(log$R$)/dT in heating and cooling cycles (defined as $T_{heating}$ and $T_{cooling}$, respectively) as follows.

$$T_c = \frac{T_{heating} + T_{cooling}}{2} \dots (1)$$

$$\Delta H = T_{heating} - T_{cooling} \dots (2)$$

For an obtained VO_2 films, the temperature dependence of the resistivity was also measured by the van der Pauw method with a Hall effect measurement system (ResiTest8300, Toyo Technica) to validate the accuracy of the measurement. The difference in the values of log (R) obtained by the two methods at the same temperature was typically less than 0.2. The transmittance spectra of the films were measured using a

UV-Vis-NIR spectrophotometer (SolidSpec-3700DUV, Shimadzu) at room temperature (~26 °C) and 100 °C using a heating stage (Mettler FP82 hotstage). The measurement error of the transmittance, which was mainly caused by baseline variation, was less than a few percent. The visible transmittance ($T_{lum}(\theta)$, 390–760 nm) and solar spectrum transmittance ($T_{sol}(\theta)$, 280–2500 nm) at a measurement temperature of θ were calculated using the following equations:

$$T_{\mathrm{lum}}(\theta) = \frac{\int \varphi_{\mathrm{lum}}(\lambda) T(\lambda,\theta) d\lambda}{\int \varphi_{\mathrm{lum}}(\lambda) d\lambda} \ldots (3)$$

$$T_{\mathrm{sol}}(\theta) = \frac{\int \varphi_{\mathrm{sol}}(\lambda) T(\lambda,\theta) d\lambda}{\int \varphi_{\mathrm{sol}}(\lambda) d\lambda} \ldots (4)$$

where $T(\lambda,\theta)$ is transmittance at wavelength λ and measurement temperature θ, $\varphi_{\mathrm{lum}}(\lambda)$ is the standard luminous efficiency function for the photopic vision of human eyes, $\varphi_{\mathrm{sol}}(\lambda)$ is the solar irradiance spectrum for an air mass of 1.5 (corresponding to the sun standing 37° above the horizon). T_{lum} and ΔT_{sol} values of the obtained films were calculated using the following equations:

$$T_{\mathrm{lum}} = \frac{T_{\mathrm{lum\,(26\,^{\circ}C)}} + T_{\mathrm{lum\,(100\,^{\circ}C)}}}{2} \ldots (5)$$

$$\Delta T_{\mathrm{sol}} = T_{\mathrm{sol\,(26\,^{\circ}C)}} - T_{\mathrm{sol\,(100\,^{\circ}C)}} \ldots (6)$$

3. Results and discussion

3.1. Appearance and phase of the films

Mist CVD was performed using a methanol or water solution of $VO(acac)_2$ to examine the effect of the solvent of the precursor solution on the resulting film. Fig. 2a and 2b show the appearance of the films deposited at 400–750 °C from methanol and water solutions, respectively. The colors of the samples show that the films were formed from methanol and water solutions at temperatures above 450 and 400 °C, respectively. The films deposited from methanol solution were gray or black, while the films deposited from water solution were brown, which is the color of monoclinic VO_2 reported in the literature [51,52].

Fig. 2c shows the XRD patterns of the samples before and after the deposition using methanol solution. After the deposition at 400 °C, the sample showed only a halo from

the quartz substrate, confirming the absence of film formation at 400 °C. In addition to the halo from the substrate, the films deposited from methanol solution at 450–650 °C showed XRD patterns corresponding to that of V_2O_3 (JCPDS 074-2037). The XRD pattern of the film deposited at 750 °C did not match any reference pattern, which indicates that an unidentified crystalline phase was formed at this temperature. Fig. 2d shows the XRD patterns of the films deposited from water solution. The sample after the deposition at 400 °C showed no diffraction peaks from the film (Fig. 2d), although the formation of the film was visually confirmed (Fig. 2b), thereby suggesting that the film was amorphous. The film deposited at 450 °C exhibited only a small peak at $2\theta = 11°$; thus, the phase of the film could not be identified. The films deposited at 550 and 650 °C exhibited the XRD patterns of VO_2 (JCPDS 072-0514), in addition to a halo from the substrates. Further, the films showed no additional peaks, thereby indicating that the films were composed of a single phase of VO_2. The film deposited at 750 °C showed no XRD peaks. However, the extension of the deposition time from 20 to 60 min resulted in the formation of a film with the XRD patterns of VO_2 (Fig. S1). This indicates that the deposition time of 20 min was significantly short to form a VO_2 film that is sufficiently thick for producing a detectable XRD pattern. In general, when mist CVD is performed at low temperatures, amorphous or unintended phases are formed because the decomposition of the precursor and the crystallization of the deposited material do not proceed sufficiently. At excessively high temperatures, the deposition rate tends to decrease owing to the increase in the re-evaporation rate of the adsorbed precursor atoms on the substrates [53–56]. The aforementioned results are consistent with these general trends and indicate that the optimal temperature for the formation of VO_2 film through mist CVD using a water solution was 550–650 °C. The reproducibility of the formation of single-phase VO_2 films was confirmed by performing the deposition under the same growth conditions several times. While VO_2 was obtained from water solution, V_2O_3 was obtained from methanol solution at 550–650 °C. The vanadium precursor employed for the film deposition was $VO(acac)_2$, which consists of V^{4+}. The XRD results indicated that the vanadium precursor was reduced to V^{3+} by methanol during the deposition process, whereas the oxidation state of the precursor was unchanged during the deposition process using water solution.

3.2. Composition and chemical states of films

XPS measurements were performed on the V_2O_3 and VO_2 films deposited at 650 °C

from methanol and water solutions, respectively, to analyze the chemical states of the elements in the films. The survey spectra (Fig. S2a) indicate the presence of V, O and contaminated C in both the films. Fig. 3a and 3c show the XPS spectra of the O1s and V2p regions. The spectra were deconvoluted into several peaks assuming the presence of oxygen with two different chemical states and vanadium with valence states ranging from +3 to +5. As shown in Table S1, the peak positions for each chemical state resulting from the deconvolution are in agreement with the reported peak positions [57–60]. The deconvolution of the V2p peaks indicates the presence of V^{3+}, V^{4+} and V^{5+} in the V_2O_3 film and V^{4+} and V^{5+} in the VO_2 film. The presence of vanadium atoms with higher oxidation numbers (V^{4+} and V^{5+} in V_2O_3, and V^{5+} in VO_2) can be attributed to the surface oxidation of the films exposed to ambient air [57,61]. No V^{3+} signal was observed in the VO_2 film, which indicates that the precursor was not reduced during the deposition process using water solution. This is consistent with the XRD pattern of the film (Fig. 2d). It should be noted that Ar^+ etching, a well-known technique for removing the surface oxidation layer, is not applicable for identifying the valence state of vanadium oxides because it results in the reduction of vanadium [62].

In the O1s region (Fig. 3a and 3c), two peaks corresponding to O in the V–O bond and O in the C–O, C=O and –OH bonds (denoted as O–C,H) were observed in both the V_2O_3 and VO_2 films. In the C1s region (Fig. 3b and 3d), two peaks corresponding to C in the C–C and C–O bonds were observed. The O–C, H, C–C and C–O peaks were not observed after Ar^+ ion etching (Fig. S2b and S2c); thus, they were assigned to surface contamination. However, another peak emerged at a binding energy slightly lower than that of the C–C bond in the C1s region for the V_2O_3 film after etching (Fig. 3b). The intensity of this peak remained almost unchanged even after increasing the etching time. The peak position (283.6 eV) was close to that of C1s in V–C [63], and thus the detection of this peak presumably indicates the presence of carbon atoms in the V_2O_3 crystal. In contrast, the VO_2 film exhibited no peaks in the C1s region after Ar^+ ion etching. This indicates that the VO_2 crystal deposited from water solution was not contaminated with carbon, except for the surface contamination layer.

3.3 Morphology of films

Fig. 4 shows the morphology of the VO_2 films deposited at 550 and 650 °C from water solution. The surface SEM images (Fig. 4a, 4b, 4e and 4f) revealed that both the films were composed of densely deposited crystal grains with a diameter of several tens of nanometers. The thicknesses of the films deposited at 550 and 650 °C were 56 and 49

nm, respectively (Fig. 4c and 4g). These are within the thickness range of 40–80 nm, where VO_2 films show a balanced combination of high visible transmittance and infrared switching efficiency [64]. The root-mean-square (RMS) roughness values of the surface of the films were determined to be 19 and 12 nm, respectively, through AFM (Fig. 4d and 4h). The film deposited at 650 °C was slightly smoother than that deposited at 550 °C.

3.4. Metal–insulator transition behavior

The temperature-dependent resistivities of the obtained films were measured to evaluate their phase transition behaviors. The resistivity of the VO_2 films deposited from water solution at 550 and 650 °C drastically decreased when heated above a certain temperature, and returned to its original value when cooled, thereby showing the typical MIT behavior (Fig. 5). In contrast, the films showing no XRD peaks of VO_2 (for instance, the film deposited at 450 °C) exhibited no MIT behavior. The resistivity of the V_2O_3 films deposited from methanol solution was nearly constant, independent of temperature, thereby confirming that no MIT occurred within the measured temperature range (Fig. S3).

The MIT characteristics of the VO_2 films, such as the magnitudes of resistivity change, phase transition temperature (T_c) and width of hysteresis loop (ΔH) determined from the resistivity–temperature curves are summarized in Table 1. T_c and ΔH values of the films were calculated from the $d(\log R)/d\theta$ curve (Fig. S4) using Equations (1) and (2), respectively. The obtained VO_2 films exhibited a resistivity change of more than two orders of magnitude. T_c and ΔH of the films were approximately 70 and 10 °C, respectively. These values are similar to those obtained by vacuum and solution processes [65,66], thus demonstrating that mist CVD is capable of producing VO_2 films with excellent phase transition properties.

Table 1 Resistivity change, transition temperature (T_c) and width of the hysteresis loop (ΔH) of the VO_2 film deposited at 550 and 650 °C using water solution.

Deposition temperature (°C)	$\log(R_{30\,°C}/R_{100\,°C})$	T_c (°C)	ΔH (°C)
550	2.1	63	11
650	2.4	73	13

3.5. Optical properties

Fig. 6 shows the transmittance spectra measured at 26 and 100 °C for the VO_2 film deposited at 650 °C from water solution. The near-infrared (NIR) transmittance of the VO_2 film decreased with an increase in temperature from 26 to 100 °C. The transmittance change was as large as 50 pp at a wavelength of 2500 nm. On the other hand, the visible transmittance was nearly constant or increased with the increasing temperature. The temperature-dependent salient change in the NIR transmittance is the typical MIT behavior of VO_2.

From the transmittance spectra, T_{lum} and ΔT_{sol} of the film were determined to be 48.1% and 5.2 pp, respectively. Gao et al. [13] reported that T_{lum} and ΔT_{sol} of VO_2 films are in the range of 10%–50% and 1–10 pp, respectively. The VO_2 film obtained in this study showed a high T_{lum} of 48.1% and a moderate ΔT_{sol} of 5.2 pp, as compared to the reported values.

Although T_{lum} and ΔT_{sol} are often used as performance indicators for smart windows, not all studies on VO_2 films have reported these values. In particular, the values for VO_2 films grown by mist CVD in previous studies are unavailable in most cases. Therefore, instead of T_{lum} and $\Delta T_{sol,}$ the transmittance at a wavelength of 550 nm ($T_{550\ nm}$) and the transmittance change at a wavelength of 2500 nm between the low and high temperatures ($\Delta T_{2500\ nm}$) [67–70] were used to compare the performance of the VO_2 films obtained in this study with those prepared through other processes. High $T_{550\ nm}$ and $\Delta T_{2500\ nm}$ are desirable for smart windows, as the former can save lighting, while the latter can effectively control heat flow [16].

Fig. 7 shows the values of $T_{550\ nm}$ and $\Delta T_{2500\ nm}$ for the non-doped VO_2 single-layer films prepared through various processes. $T_{550\ nm}$ and $\Delta T_{2500\ nm}$ of the VO_2 film obtained in this study were 47.8% and 57.6 pp, respectively. Compared to the values for previously reported mist-CVD-grown VO_2 films, $T_{550\ nm}$ of the film obtained in this study was nearly the highest and its $\Delta T_{2500\ nm}$ was significantly higher.

Some VO_2 films prepared by other processes have higher values of either $T_{550\ nm}$ or $\Delta T_{2500\ nm}$ than the VO_2 film obtained in this study; however, we did not find any studies reporting higher values of both the parameters. As many studies have pointed out, $T_{550\ nm}$ and $\Delta T_{2500\ nm}$ show a trade-off relationship [13], assuming the same quality of VO_2. For example, depending on the thickness of VO_2, one of these values will increase at the expense of the other. Therefore, among the reported VO_2 films, those with the data points ($T_{550\ nm}$, $\Delta T_{2500\ nm}$) located within the zone connecting the highest $\Delta T_{2500\ nm}$ and $T_{550\ nm}$ (the blue region) in Fig. 7 can be considered to be of similar high quality. The VO_2 film

obtained in this study was located within this zone, thereby exhibiting excellent smart window properties comparable to those of high-quality VO_2 films fabricated by other methods.

The enhancement in the quality of the mist-CVD-grown VO_2 films can be attributed to the use of water as the solvent of the precursor solution; previous films were formed from ethanol-based precursor solutions. According to previous studies, water vapor atmosphere is suitable for stabilizing vanadium in the tetravalent state [48,49]. It is known that the performance of smart windows decreases when V^{3+} and V^{5+} contaminate VO_2 [43–45]. The excellent thermochromic properties of the VO_2 film obtained in this study can be attributed to the suppression of V^{3+} and V^{5+} contamination during the deposition by the water solution used in the mist CVD process. Note that, although V^{5+} was detected in the VO_2 film by XPS (Fig. 3a and 3c), it does not indicate the presence of V^{5+} in the bulk of the film because XPS only detects the surface elements.

4. Conclusion

High-quality VO_2 films were fabricated through a mist CVD method, which can deposit films at low cost and with high productivity. VO_2 and V_2O_3 films were obtained using water-based and methanol-based precursor solutions, respectively. The obtained VO_2 film showed a high visible transmittance and a large infrared transmittance change compared to those of previously reported mist-CVD-grown VO_2 films. These values are similar to those of high-quality VO_2 deposited by solution and vacuum processes, demonstrating that mist CVD is a promising method for the fabrication of VO_2-based smart windows. However, the VO_2 deposition temperature of 550–650 °C is significantly high for coating on inexpensive soda-lime glass, which is commonly used for windows. In future work, the deposition temperature of VO_2 is expected to be lower in mist CVD.

Acknowledgements

The authors would like to thank Mr. R. Kumazawa of the Toray Research Center for the UV-VIS-NIR measurements. This work was partly supported by KAKENHI (Grant No. 18K18943).

References

[1] K. Valadi, S. Gharibi, R. Taheri-Ledari, S. Akin, A. Maleki, A.E. Shalan, Metal oxide electron transport materials for perovskite solar cells: a review, Environ. Chem. Lett. 19 (2021) 2185–2207. https://doi.org/10.1007/s10311-020-01171-x.

[2] D. Pugliese, A. Lamberti, F. Bella, A. Sacco, S. Bianco, E. Tresso, TiO_2 nanotubes as flexible photoanode for back-illuminated dye-sensitized solar cells with hemi-squaraine organic dye and iodine-free transparent electrolyte, Org. Electron. 15 (2014) 3715–3722. https://doi.org/10.1016/j.orgel.2014.10.018.

[3] Z. Yao, W. Duan, P. Steuter, J. Hüpkes, A. Lambertz, K. Bittkau, M. Pomaska, D. Qiu, K. Qiu, Z. Wu, H. Shen, U. Rau, K. Ding, Influence of Oxygen on Sputtered Titanium-Doped Indium Oxide Thin Films and Their Application in Silicon Heterojunction Solar Cells, Sol. RRL. 5 (2021) 2000501. https://doi.org/10.1002/solr.202000501.

[4] T. Sugiura, S. Matsumoto, N. Nakano, Numerical analysis of tunnel oxide passivated contact solar cell performances for dielectric thin film materials and bulk properties, Sol. Energy. 214 (2021) 205–213. https://doi.org/10.1016/j.solener.2020.11.032.

[5] L. Fagiolari, M. Bonomo, A. Cognetti, G. Meligrana, C. Gerbaldi, C. Barolo, F. Bella, Photoanodes for Aqueous Solar Cells: Exploring Additives and Formulations Starting from a Commercial TiO_2 Paste, ChemSusChem. 13 (2020) 6562–6573. https://doi.org/10.1002/cssc.202001898.

[6] Y. Chen, X. Chen, Y. Zhang, A Comprehensive Review on Metal-Oxide Nanocomposites for High-Performance Lithium-Ion Battery Anodes, Energy & Fuels. 35 (2021) 6420–6442. https://doi.org/10.1021/acs.energyfuels.1c00315.

[7] A. Massaro, A.B. Muñoz-García, P. Maddalena, F. Bella, G. Meligrana, C. Gerbaldi, M. Pavone, First-principles study of Na insertion at TiO_2 anatase surfaces: New hints for Na-ion battery design, Nanoscale Adv. 2 (2020) 2745–2751. https://doi.org/10.1039/d0na00230e.

[8] B. Miccoli, V. Cauda, A. Bonanno, A. Sanginario, K. Bejtka, F. Bella, M. Fontana, D. Demarchi, One-Dimensional ZnO/Gold Junction for Simultaneous and Versatile Multisensing Measurements, Sci. Rep. 6 (2016) 1–10. https://doi.org/10.1038/srep29763.

[9] X. Cao, T. Chang, Z. Shao, F. Xu, H. Luo, P. Jin, Challenges and Opportunities toward Real Application of VO_2-Based Smart Glazing, Matter. 2 (2020) 862–881. https://doi.org/10.1016/j.matt.2020.02.009.

[10] A. Mehmood, X. Long, A.A. Haidry, X. Zhang, Trends in sputter deposited tungsten oxide structures for electrochromic applications: A review, Ceram. Int. 46 (2020) 23295–23313. https://doi.org/10.1016/j.ceramint.2020.06.035.
[11] S.M. Babulanam, T.S. Eriksson, G.A. Niklasson, C.G. Granqvist, Thermochromic VO_2 films for energy-efficient windows, Sol. Energy Mater. 16 (1987) 347–363. https://doi.org/10.1016/0165-1633(87)90029-3.
[12] G.V. Jorgenson, J.C. Lee, Doped vanadium oxide for optical switching films, Sol. Energy Mater. 14 (1986) 205–214. https://doi.org/10.1016/0165-1633(86)90047-X.
[13] Y. Gao, H. Luo, Z. Zhang, L. Kang, Z. Chen, J. Du, M. Kanehira, C. Cao, Nanoceramic VO_2 thermochromic smart glass: A review on progress in solution processing, Nano Energy. 1 (2012) 221–246. https://doi.org/10.1016/j.nanoen.2011.12.002.
[14] M. Li, S. Magdassi, Y. Gao, Y. Long, Hydrothermal Synthesis of VO_2 Polymorphs: Advantages, Challenges and Prospects for the Application of Energy Efficient Smart Windows, Small. 13 (2017) 1701147. https://doi.org/10.1002/smll.201701147.
[15] Y.S. Chen, H.C. Ho, Y.C. Lai, T. Nagao, C.H. Hsueh, Thermochromic vanadium dioxide film on textured silica substrate for smart window with enhanced visible transmittance and tunable infrared radiation, Infrared Phys. Technol. 102 (2019) 103019. https://doi.org/10.1016/j.infrared.2019.103019.
[16] Y. Cui, Y. Ke, C. Liu, Z. Chen, N. Wang, L. Zhang, Y. Zhou, S. Wang, Y. Gao, Y. Long, Thermochromic VO_2 for Energy-Efficient Smart Windows, Joule. 2 (2018) 1707–1746. https://doi.org/10.1016/j.joule.2018.06.018.
[17] S. Wang, M. Liu, L. Kong, Y. Long, X. Jiang, A. Yu, Recent progress in VO_2 smart coatings: Strategies to improve the thermochromic properties, Prog. Mater. Sci. 81 (2016) 1–54. https://doi.org/10.1016/j.pmatsci.2016.03.001.
[18] F.J. Morin, Oxides which show a metal-to-insulator transition at the Neel temperature, Phys. Rev. Lett. 3 (1959) 34–36. https://doi.org/10.1103/PhysRevLett.3.34.
[19] F. Béteille, J. Livage, Optical Switching in VO_2 Thin Films, J. Sol-Gel Sci. Technol. 13 (1998) 915–921. https://doi.org/10.1023/A:1008679408509.
[20] A.S. Barker, H.W. Verleur, H.J. Guggenheim, Infrared optical properties of vanadium dioxide above and below the transition temperature, Phys. Rev. Lett. 17 (1966) 1286–1289. https://doi.org/10.1103/PhysRevLett.17.1286.
[21] Z. Chen, Y. Gao, L. Kang, C. Cao, S. Chen, H. Luo, Fine crystalline VO_2

nanoparticles: synthesis, abnormal phase transition temperatures and excellent optical properties of a derived VO2 nanocomposite foil, J. Mater. Chem. A. 2 (2014) 2718. https://doi.org/10.1039/c3ta14612j.

[22] S.R. Popuri, M. Miclau, A. Artemenko, C. Labrugere, A. Villesuzanne, M. Pollet, Rapid Hydrothermal Synthesis of VO_2 (B) and Its Conversion to Thermochromic VO_2 (M1), Inorg. Chem. 52 (2013) 4780–4785. https://doi.org/10.1021/ic301201k.

[23] B.-G. Chae, H.-T. Kim, S.-J. Yun, B.-J. Kim, Y.-W. Lee, D.-H. Youn, K.-Y. Kang, Highly Oriented VO_2 Thin Films Prepared by Sol-Gel Deposition, Electrochem. Solid-State Lett. 9 (2006) C12. https://doi.org/10.1149/1.2135430.

[24] L. Mathevula, B.D. Ngom, L. Kotsedi, P. Sechogela, T.B. Doyle, M. Ghouti, M. Maaza, Thermochromic VO_2 on Zinnwaldite Mica by pulsed laser deposition, Appl. Surf. Sci. 314 (2014) 476–480. https://doi.org/10.1016/j.apsusc.2014.07.035.

[25] P. Jin, S. Tanemura, Formation and Thermochromism of VO_2 Films Deposited by RF Magnetron Sputtering at Low Substrate Temperature, Jpn. J. Appl. Phys. 33 (1994) 1478–1483. https://doi.org/10.1143/JJAP.33.1478.

[26] E. Gagaoudakis, E. Aperathitis, G. Michail, M. Panagopoulou, D. Katerinopoulou, V. Binas, Y.S. Raptis, G. Kiriakidis, Low-temperature rf sputtered VO_2 thin films as thermochromic coatings for smart glazing systems, Sol. Energy. 165 (2018) 115–121. https://doi.org/10.1016/j.solener.2018.03.010.

[27] P. Dagur, A.U. Mane, S.A. Shivashankar, Thin films of VO_2 on glass by atomic layer deposition: microstructure and electrical properties, J. Cryst. Growth. 275 (2005) e1223–e1228. https://doi.org/10.1016/j.jcrysgro.2004.11.144.

[28] T. Maruyama, Y. Ikuta, Vanadium dioxide thin films prepared by chemical vapour deposition from vanadium(III) acetylacetonate, J. Mater. Sci. 28 (1993) 5073–5078. https://doi.org/10.1007/BF00361182.

[29] T.D. Manning, I.P. Parkin, M.E. Pemble, D. Sheel, D. Vernardou, Intelligent Window Coatings: Atmospheric Pressure Chemical Vapor Deposition of Tungsten-Doped Vanadium Dioxide, Chem. Mater. 16 (2004) 744–749. https://doi.org/10.1021/cm034905y.

[30] T. Ikenoue, S. Sakamoto, Y. Inui, Fabrication and characteristics of p-type Cu_2O thin films by ultrasonic spray-assisted mist CVD method, Jpn. J. Appl. Phys. 53 (2014) 05FF06. https://doi.org/10.7567/JJAP.53.05FF06.

[31] D. Shinohara, S. Fujita, Heteroepitaxy of corundum-structured α-Ga_2O_3 thin films on α-Al_2O_3 substrates by ultrasonic mist chemical vapor deposition, Jpn. J.

Appl. Phys. 47 (2008) 7311–7313. https://doi.org/10.1143/JJAP.47.7311.
[32] T. Kawaharamura, H. Nishinaka, S. Fujita, Growth of crystalline zinc oxide thin films by fine-channel-mist chemical vapor deposition, Jpn. J. Appl. Phys. 47 (2008) 4669–4675. https://doi.org/10.1143/JJAP.47.4669.
[33] H. Nishinaka, T. Kawaharamura, S. Fujita, Low-temperature growth of ZnO thin films by linear source ultrasonic spray chemical vapor deposition, Jpn. J. Appl. Phys. 46 (2007) 6811–6813. https://doi.org/10.1143/JJAP.46.6811.
[34] H. Ito, K. Kaneko, S. Fujita, Growth and band gap control of corundum-structured α-$(AlGa)_2O_3$ thin films on sapphire by spray-assisted mist chemical vapor deposition, Jpn. J. Appl. Phys. 51 (2012) 100207. https://doi.org/10.1143/JJAP.51.100207.
[35] T. Uchida, T. Kawaharamura, K. Shibayama, T. Hiramatsu, H. Orita, S. Fujita, Mist chemical vapor deposition of aluminum oxide thin films for rear surface passivation of crystalline silicon solar cells, Appl. Phys. Express. 7 (2014) 021303. https://doi.org/10.7567/APEX.7.021303.
[36] J.G. Lu, T. Kawaharamura, H. Nishinaka, Y. Kamada, T. Ohshima, S. Fujita, ZnO-based thin films synthesized by atmospheric pressure mist chemical vapor deposition, J. Cryst. Growth. 299 (2007) 1–10. https://doi.org/10.1016/j.jcrysgro.2006.10.251.
[37] C. Piccirillo, R. Binions, I.P. Parkin, Nb-Doped VO_2 Thin Films Prepared by Aerosol-Assisted Chemical Vapour Deposition, Eur. J. Inorg. Chem. 2007 (2007) 4050–4055. https://doi.org/10.1002/ejic.200700284.
[38] C. Piccirillo, R. Binions, I.P. Parkin, Synthesis and characterisation of W-doped VO_2 by Aerosol Assisted Chemical Vapour Deposition, Thin Solid Films. 516 (2008) 1992–1997. https://doi.org/10.1016/j.tsf.2007.06.009.
[39] C. Piccirillo, R. Binions, I.P. Parkin, Synthesis and functional properties of vanadium oxides: V_2O_3, VO_2, and V_2O_5 deposited on glass by aerosol-assisted CVD, Chem. Vap. Depos. 13 (2007) 145–151. https://doi.org/10.1002/cvde.200606540.
[40] P. Kiri, M.E.A. Warwick, I. Ridley, R. Binions, Fluorine doped vanadium dioxide thin films for smart windows, Thin Solid Films. 520 (2011) 1363–1366. https://doi.org/10.1016/j.tsf.2011.01.401.
[41] M.E.A. Warwick, R. Binions, Thermochromic vanadium dioxide thin films from electric field assisted aerosol assisted chemical vapour deposition, Sol. Energy Mater. Sol. Cells. 143 (2015) 592–600. https://doi.org/10.1016/j.solmat.2015.01.025.

[42] I. Top, R. Binions, M.E.A. Warwick, C.W. Dunnill, M. Holdynski, I. Abrahams, VO_2/TiO_2 bilayer films for energy efficient windows with multifunctional properties, J. Mater. Chem. C. 6 (2018) 4485–4493. https://doi.org/10.1039/C8TC00835C.
[43] C. Wu, F. Feng, Y. Xie, Design of vanadium oxide structures with controllable electrical properties for energy applications, Chem. Soc. Rev. 42 (2013) 5157. https://doi.org/10.1039/c3cs35508j.
[44] Z. Yang, C. Ko, S. Ramanathan, Oxide Electronics Utilizing Ultrafast Metal-Insulator Transitions, Annu. Rev. Mater. Res. 41 (2011) 337–367. https://doi.org/10.1146/annurev-matsci-062910-100347.
[45] T.W. Chiu, K. Tonooka, N. Kikuchi, Influence of oxygen pressure on the structural, electrical and optical properties of VO_2 thin films deposited on ZnO/glass substrates by pulsed laser deposition, in: Thin Solid Films, Elsevier, 2010: pp. 7441–7444. https://doi.org/10.1016/j.tsf.2010.05.019.
[46] J.-Y. Bae, J. Park, H.Y. Kim, H.-S. Kim, J.-S. Park, Facile Route to the Controlled Synthesis of Tetragonal and Orthorhombic SnO_2 Films by Mist Chemical Vapor Deposition, ACS Appl. Mater. Interfaces. 7 (2015) 12074–12079. https://doi.org/10.1021/acsami.5b02251.
[47] D.-H. Kim, H.-J. Jeong, J. Park, J.-S. Park, The effect of solvent water content on the dielectric properties of Al_2O_3 films grown by atmospheric pressure mist-CVD, Ceram. Int. 44 (2018) 459–463. https://doi.org/10.1016/j.ceramint.2017.09.198.
[48] H. Ren, B. Li, X. Zhou, S. Chen, Y. Li, C. Hu, J. Tian, G. Zhang, Y. Pan, C. Zou, Wafer-size VO_2 film prepared by water-vapor oxidant, Appl. Surf. Sci. 525 (2020) 146642. https://doi.org/10.1016/j.apsusc.2020.146642.
[49] W. Liang, M. Gao, C. Lu, Z. Zhang, C.H. Chan, L. Zhuge, J. Dai, H. Yang, C. Chen, B.H. Park, Q. Jia, Y. Lin, Enhanced Metal-Insulator Transition Performance in Scalable Vanadium Dioxide Thin Films Prepared Using a Moisture-Assisted Chemical Solution Approach, ACS Appl. Mater. Interfaces. 10 (2018) 8341–8348. https://doi.org/10.1021/acsami.7b18533.
[50] Y. Matamura, T. Ikenoue, M. Miyake, T. Hirato, Mist chemical vapor deposition of MoO_2 thin films, J. Cryst. Growth. 548 (2020) 125862. https://doi.org/10.1016/j.jcrysgro.2020.125862.
[51] J. Zheng, S. Bao, P. Jin, TiO_2(R)/VO_2(M)/TiO_2(A) multilayer film as smart window: Combination of energy-saving, antifogging and self-cleaning functions, Nano Energy. 11 (2015) 136–145. https://doi.org/10.1016/j.nanoen.2014.09.023.

[52] Y. Gao, S. Wang, H. Luo, L. Dai, C. Cao, Y. Liu, Z. Chen, M. Kanehira, Enhanced chemical stability of VO_2 nanoparticles by the formation of SiO_2/VO_2 core/shell structures and the application to transparent and flexible VO_2-based composite foils with excellent thermochromic properti, Energy Environ. Sci. 5 (2012) 6104. https://doi.org/10.1039/c2ee02803d.

[53] T. Oshima, T. Nakazono, A. Mukai, A. Ohtomo, Epitaxial growth of γ-Ga_2O_3 films by mist chemical vapor deposition, J. Cryst. Growth. 359 (2012) 60–63. https://doi.org/10.1016/j.jcrysgro.2012.08.025.

[54] T. Ikenoue, J. Inoue, M. Miyake, T. Hirato, Epitaxial growth of undoped and Li-doped NiO thin films on α-Al_2O_3 substrates by mist chemical vapor deposition, J. Cryst. Growth. 507 (2019) 379–383. https://doi.org/10.1016/j.jcrysgro.2018.11.032.

[55] X. Zhao, J. Cheng, Atmospheric preparation of ZnO thin films by mist chemical vapor deposition for spray-coated organic solar cells, J. Mater. Sci. Mater. Electron. 27 (2016) 2676–2681. https://doi.org/10.1007/s10854-015-4076-y.

[56] Z. Sun, D. Oka, T. Fukumura, Epitaxial Growth of β-Bi_2O_3 Thin Films and Particles with Mist Chemical Vapor Deposition, Cryst. Growth Des. 19 (2019) 7170–7174. https://doi.org/10.1021/acs.cgd.9b01033.

[57] G. Silversmit, D. Depla, H. Poelman, G.B. Marin, R. De Gryse, Determination of the V2p XPS binding energies for different vanadium oxidation states (V^{5+} to V^{0+}), J. Electron Spectros. Relat. Phenomena. 135 (2004) 167–175. https://doi.org/10.1016/j.elspec.2004.03.004.

[58] V. Bondarenka, V. Jasulaitienė, R. Sereika, A. Stirkė, Sol–gel synthesis and XPS study of vanadium pentoxide xerogels intercalated with glucose, J. Sol-Gel Sci. Technol. 71 (2014) 385–390. https://doi.org/10.1007/s10971-014-3385-6.

[59] E. Hryha, E. Rutqvist, L. Nyborg, Stoichiometric vanadium oxides studied by XPS, Surf. Interface Anal. 44 (2012) 1022–1025. https://doi.org/10.1002/sia.3844.

[60] J.K. Tripathi, T.J. Novakowski, A. Hassanein, Tuning surface porosity on vanadium surface by low energy He^+ ion irradiation, Appl. Surf. Sci. 378 (2016) 63–72. https://doi.org/10.1016/j.apsusc.2016.03.196.

[61] F. Ureña-Begara, A. Crunteanu, J.-P. Raskin, Raman and XPS characterization of vanadium oxide thin films with temperature, Appl. Surf. Sci. 403 (2017) 717–727. https://doi.org/10.1016/j.apsusc.2017.01.160.

[62] G. Silversmit, D. Depla, H. Poelman, G.B. Marin, R. De Gryse, An XPS study on the surface reduction of V_2O_5(001) induced by Ar^+ ion bombardment, Surf. Sci.

600 (2006) 3512–3517. https://doi.org/10.1016/j.susc.2006.07.006.
[63] A. Pajares, H. Prats, A. Romero, F. Viñes, P.R. de la Piscina, R. Sayós, N. Homs, F. Illas, Critical effect of carbon vacancies on the reverse water gas shift reaction over vanadium carbide catalysts, Appl. Catal. B Environ. 267 (2020) 118719. https://doi.org/10.1016/j.apcatb.2020.118719.
[64] Z. Zhang, Y. Gao, Z. Chen, J. Du, C. Cao, L. Kang, H. Luo, Thermochromic VO_2 thin films: Solution-based processing, improved optical properties, and lowered phase transformation temperature, Langmuir. 26 (2010) 10738–10744. https://doi.org/10.1021/la100515k.
[65] T.. Hanlon, R.. Walker, J.. Coath, M.. Richardson, Comparison between vanadium dioxide coatings on glass produced by sputtering, alkoxide and aqueous sol–gel methods, Thin Solid Films. 405 (2002) 234–237. https://doi.org/10.1016/S0040-6090(01)01753-9.
[66] M. Zhu, H. Wang, C. Li, H. Qi, D. Zhang, W. Lv, Thickness-modulated thermochromism of vanadium dioxide thin films grown by magnetron sputtering, Surf. Coatings Technol. 359 (2019) 396–402. https://doi.org/10.1016/j.surfcoat.2018.12.077.
[67] D. Zhang, M. Zhu, Y. Liu, K. Yang, G. Liang, Z. Zheng, X. Cai, P. Fan, High performance VO_2 thin films growth by DC magnetron sputtering at low temperature for smart energy efficient window application, J. Alloys Compd. 659 (2016) 198–202. https://doi.org/10.1016/j.jallcom.2015.11.047.
[68] J. Vlček, D. Kolenatý, J. Houška, T. Kozák, R. Čerstvý, Controlled reactive HiPIMS—effective technique for low-temperature (300 °C) synthesis of VO_2 films with semiconductor-to-metal transition, J. Phys. D. Appl. Phys. 50 (2017) 38LT01. https://doi.org/10.1088/1361-6463/aa8356.
[69] M. Xygkis, E. Gagaoudakis, L. Zouridi, O. Markaki, E. Aperathitis, K. Chrissopoulou, G. Kiriakidis, V. Binas, Thermochromic Behavior of VO_2/Polymer Nanocomposites for Energy Saving Coatings, Coatings. 9 (2019) 163. https://doi.org/10.3390/coatings9030163.
[70] L. Zhao, L. Miao, S. Tanemura, J. Zhou, L. Chen, X. Xiao, G. Xu, A low cost preparation of VO_2 thin films with improved thermochromic properties from a solution-based process, Thin Solid Films. 543 (2013) 157–161. https://doi.org/10.1016/j.tsf.2012.11.154.
[71] H. Kim, N. Charipar, E. Breckenfeld, A. Rosenberg, A. Piqué, Active terahertz metamaterials based on the phase transition of VO_2 thin films, Thin Solid Films. 596 (2015) 45–50. https://doi.org/10.1016/j.tsf.2015.07.062.

[72] C. Ji, Z. Wu, X. Wu, J. Wang, J. Gou, Z. Huang, H. Zhou, W. Yao, Y. Jiang, Al-doped VO_2 films as smart window coatings: Reduced phase transition temperature and improved thermochromic performance, Sol. Energy Mater. Sol. Cells. 176 (2018) 174–180. https://doi.org/10.1016/j.solmat.2017.11.026.

[73] S. Long, X. Cao, G. Sun, N. Li, T. Chang, Z. Shao, P. Jin, Effects of V_2O_3 buffer layers on sputtered VO_2 smart windows: Improved thermochromic properties, tunable width of hysteresis loops and enhanced durability, Appl. Surf. Sci. 441 (2018) 764–772. https://doi.org/10.1016/j.apsusc.2018.02.083.

[74] X. Wu, Z. Wu, H. Zhang, R. Niu, Q. He, C. Ji, J. Wang, Y. Jiang, Enhancement of VO_2 thermochromic properties by Si doping, Surf. Coatings Technol. 276 (2015) 248–253. https://doi.org/10.1016/j.surfcoat.2015.07.007.

[75] M.K. Dietrich, B.G. Kramm, M. Becker, B.K. Meyer, A. Polity, P.J. Klar, Influence of doping with alkaline earth metals on the optical properties of thermochromic VO_2, J. Appl. Phys. 117 (2015) 185301. https://doi.org/10.1063/1.4919433.

[76] M. Jiang, S. Bao, X. Cao, Y. Li, S. Li, H. Zhou, H. Luo, P. Jin, Improved luminous transmittance and diminished yellow color in VO_2 energy efficient smart thin films by Zn doping, Ceram. Int. 40 (2014) 6331–6334. https://doi.org/10.1016/j.ceramint.2013.10.083.

[77] H. Guan, D. Zhang, Y. Yang, Y. Liu, A. Zhong, Q. He, J. Qi, P. Fan, A Novel Method for Notable Reducing Phase Transition Temperature of VO_2 Films for Smart Energy Efficient Windows, Nanomaterials. 10 (2019) 58. https://doi.org/10.3390/nano10010058.

[78] S. Long, X. Cao, Y. Wang, T. Chang, N. Li, L. Jin, L. Ma, F. Xu, G. Sun, P. Jin, Karst landform-like VO_2 single layer solution: Controllable morphology and excellent optical performance for smart glazing applications, Sol. Energy Mater. Sol. Cells. 209 (2020) 110449. https://doi.org/10.1016/j.solmat.2020.110449.

[79] M.J. Miller, J. Wang, Influence of grain size on transition temperature of thermochromic VO_2, J. Appl. Phys. 117 (2015) 034307. https://doi.org/10.1063/1.4906122.

[80] H. Koo, H. You, K.-E. Ko, O.-J. Kwon, S.-H. Chang, C. Park, Thermochromic properties of VO_2 thin film on SiN_x buffered glass substrate, Appl. Surf. Sci. 277 (2013) 237–241. https://doi.org/10.1016/j.apsusc.2013.04.031.

[81] T. Lin, Y. Zhang, D. Zheng, The ultrathin VO2(M) film with ultrahigh visible transmittance synthesized on the quartz glass substrate by HiPIMS, Vacuum. 156 (2018) 449–455. https://doi.org/10.1016/j.vacuum.2018.08.008.

[82] J. Kim, T. Ejiri, M. Sugiyama, Investigation of VO_2 directly deposited on a glass substrate using RF sputtering for a smart window, Jpn. J. Appl. Phys. 59 (2020) 105506. https://doi.org/10.35848/1347-4065/abbb1d.
[83] G. Fu, A. Polity, N. Volbers, B.K. Meyer, Annealing effects on VO_2 thin films deposited by reactive sputtering, Thin Solid Films. 515 (2006) 2519–2522. https://doi.org/10.1016/j.tsf.2006.04.025.
[84] H.-C. Ho, Y.-C. Lai, K. Chen, T.D. Dao, C.-H. Hsueh, T. Nagao, High quality thermochromic VO_2 films prepared by magnetron sputtering using V_2O_5 target with in situ annealing, Appl. Surf. Sci. 495 (2019) 143436. https://doi.org/10.1016/j.apsusc.2019.07.178.
[85] B. Zhu, H. Tao, X. Zhao, Effect of buffer layer on thermochromic performances of VO_2 films fabricated by magnetron sputtering, Infrared Phys. Technol. 75 (2016) 22–25. https://doi.org/10.1016/j.infrared.2016.01.004.
[86] Y. Shigesato, M. Enomoto, H. Odaka, Thermochromic VO_2 Films Deposited by RF Magnetron Sputtering Using V_2O_3 or V_2O_5 Targets, Jpn. J. Appl. Phys. 39 (2000) 6016–6024. https://doi.org/10.1143/JJAP.39.6016.
[87] Y. Yang, X. Cao, G. Sun, S. Long, T. Chang, X. Li, P. Jin, Transmittance change with thickness for polycrystalline VO_2 films deposited at room temperature, J. Alloys Compd. 791 (2019) 648–654. https://doi.org/10.1016/j.jallcom.2019.03.278.
[88] X. Lv, Y. Cao, L. Yan, Y. Li, L. Song, Atomic layer deposition of VO_2 films with Tetrakis-dimethyl-amino vanadium (IV) as vanadium precursor, Appl. Surf. Sci. 396 (2017) 214–220. https://doi.org/10.1016/j.apsusc.2016.10.044.
[89] D. Malarde, M.J. Powell, R. Quesada-Cabrera, R.L. Wilson, C.J. Carmalt, G. Sankar, I.P. Parkin, R.G. Palgrave, Optimized Atmospheric-Pressure Chemical Vapor Deposition Thermochromic VO_2 Thin Films for Intelligent Window Applications, ACS Omega. 2 (2017) 1040–1046. https://doi.org/10.1021/acsomega.7b00042.
[90] S. Ji, F. Zhang, P. Jin, Preparation of high performance pure single phase VO_2 nanopowder by hydrothermally reducing the V_2O_5 gel, Sol. Energy Mater. Sol. Cells. 95 (2011) 3520–3526. https://doi.org/10.1016/j.solmat.2011.08.015.
[91] W. Li, S. Ji, Y. Li, A. Huang, H. Luo, P. Jin, Synthesis of VO_2 nanoparticles by a hydrothermal-assisted homogeneous precipitation approach for thermochromic applications, RSC Adv. 4 (2014) 13026–13033. https://doi.org/10.1039/c3ra47666a.
[92] L. Dai, S. Chen, J. Liu, Y. Gao, J. Zhou, Z. Chen, C. Cao, H. Luo, M. Kanehira,

F-doped VO_2 nanoparticles for thermochromic energy-saving foils with modified color and enhanced solar-heat shielding ability, Phys. Chem. Chem. Phys. 15 (2013) 11723–11729. https://doi.org/10.1039/c3cp51359a.

[93] Z. Zhao, Y. Liu, D. Wang, C. Ling, Q. Chang, J. Li, Y. Zhao, H. Jin, Sn dopants improve the visible transmittance of VO_2 films achieving excellent thermochromic performance for smart window, Sol. Energy Mater. Sol. Cells. 209 (2020) 110443. https://doi.org/10.1016/j.solmat.2020.110443.

[94] N. Wang, M. Duchamp, R.E. Dunin-Borkowski, S. Liu, X. Zeng, X. Cao, Y. Long, Terbium-Doped VO_2 Thin Films: Reduced Phase Transition Temperature and Largely Enhanced Luminous Transmittance, Langmuir. 32 (2016) 759–764. https://doi.org/10.1021/acs.langmuir.5b04212.

Figure captions

Fig. 1 Schematic illustration of a hot-wall mist CVD system.

Fig. 2 (a, b) Photographs and (c, d) XRD patterns of the substrates before and after film deposition at 400–750 °C using (a, c) methanol and (b, d) water solutions of $VO(acac)_2$.

Fig. 3 (a,c) O1s and V2p spectra of the films deposited at 650 °C from (a) methanol and (c) water solutions. (b,d) Deconvolution of C1s spectra for the films deposited at 650 °C from the (b) methanol and (d) water solutions before and after Ar^+ ion etching.

Fig. 4 Surface and cross-sectional SEM and AFM images of the VO_2 films deposited (a–d) at 550 and (e–h) at 650 °C.

Fig. 5 Electric resistance of the films deposited from water solution at 550–650 °C as a function of temperature.

Fig. 6 Transmittance spectra measured at 26 and 100 °C for the VO_2 films deposited at 650 °C.

Fig. 7 Visible transmittance at a wavelength of 550 nm ($T_{550\,nm}$) and infrared transmittance difference at a wavelength of 2500 nm between low (26 °C) and high temperature states (100 °C) ($\Delta T_{2500\,nm}$) of VO_2 fabricated through vacuum processes (●) [15,16,57,61–78], atmospheric pressure process (▼) [89], solution processes (◆) [64,70,90–94] and the mist CVD method (★) [37–42].

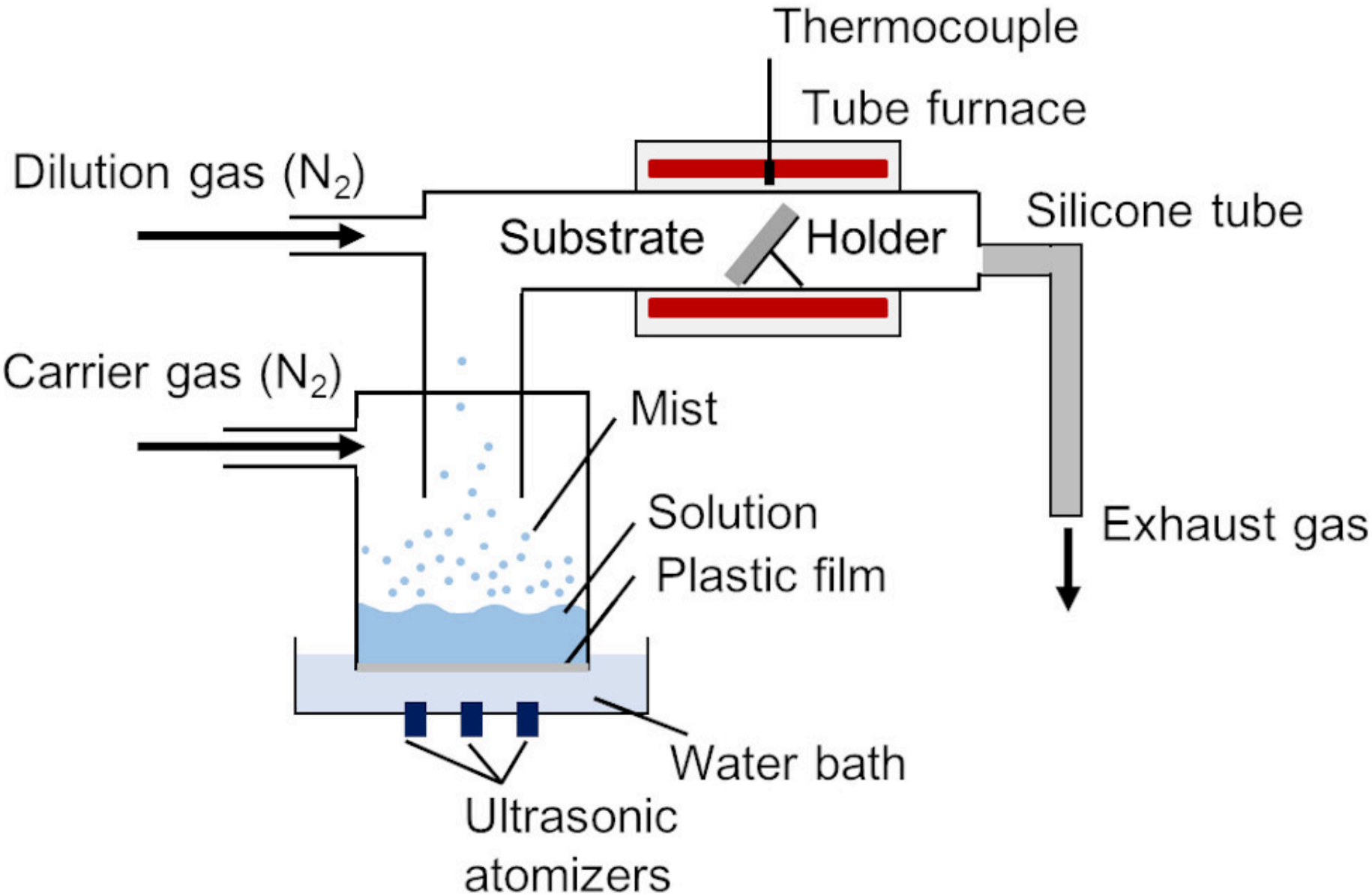
Thermocouple
Tube furnace
Dilution gas (N_2)
Substrate
Holder
Silicone tube
Carrier gas (N_2)
Mist
Solution
Plastic film
Exhaust gas
Water bath
Ultrasonic
atomizers

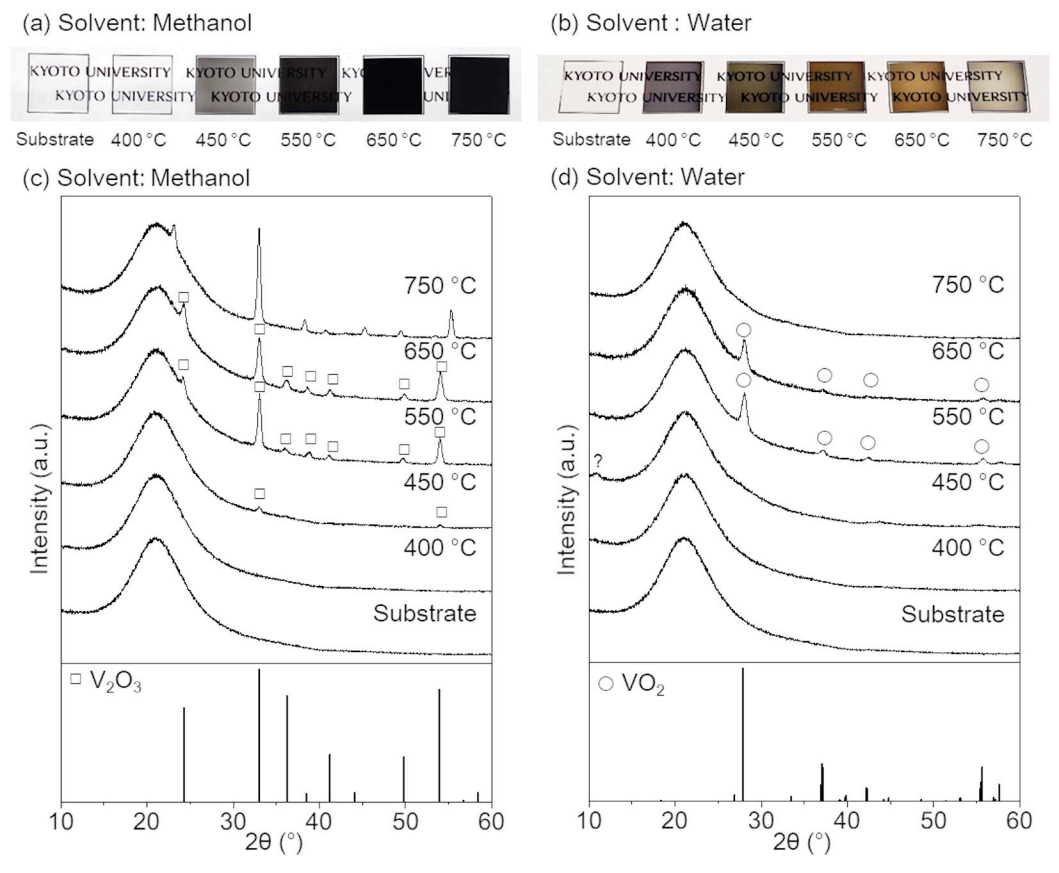
(a) Solvent: Methanol
(b) Solvent : Water
Substrate 400 °C 450 °C 550 °C 650 °C 750 °C
Substrate 400 °C 450 °C 550 °C 650 °C 750 °C
(c) Solvent: Methanol
(d) Solvent: Water
750 °C
650 °C
550 °C
450 °C
400 °C
Substrate
Intensity (a.u.)
□ V2O3
○ VO2
?
10 20 30 40 50 60
2θ (°)

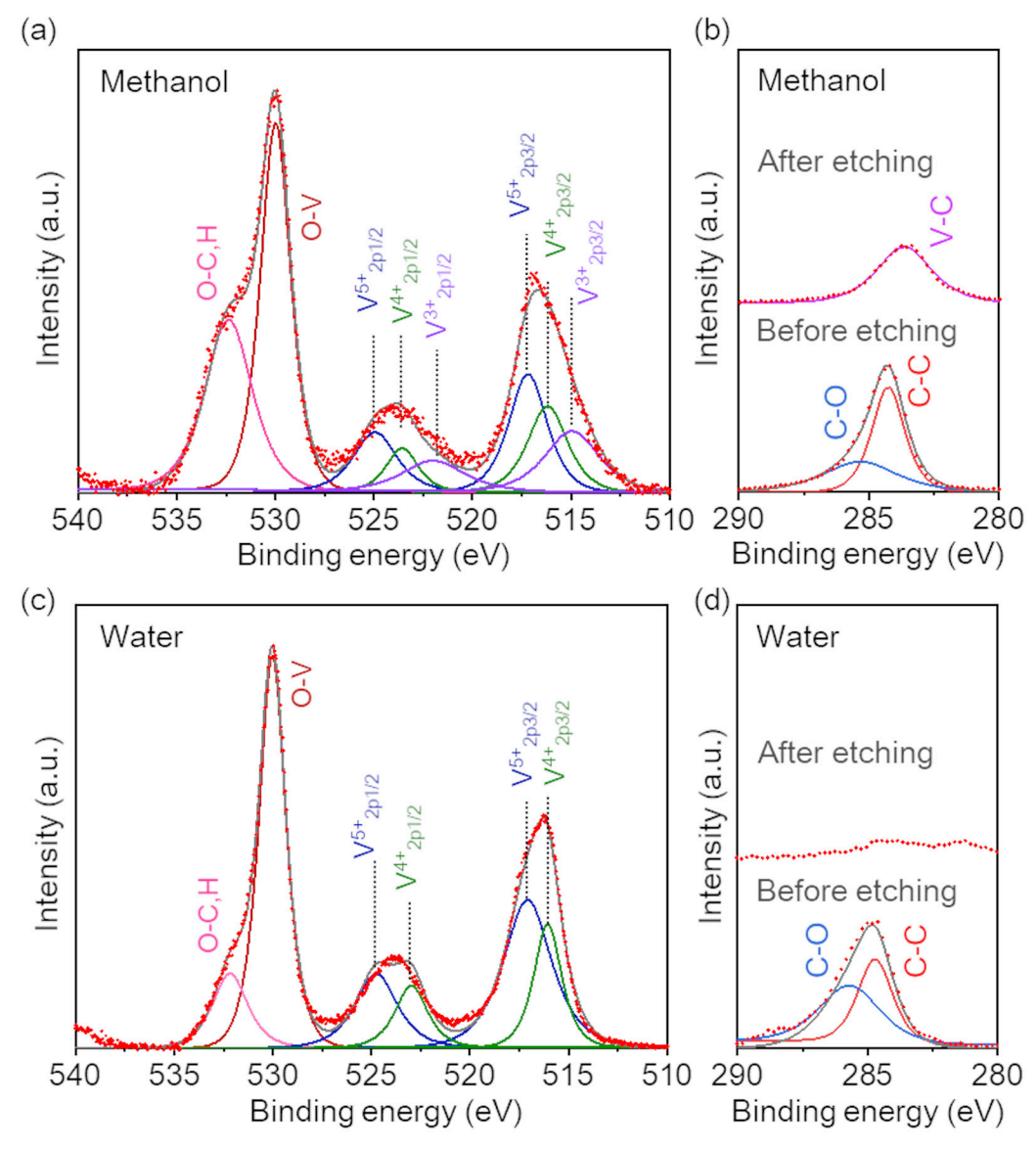
(a)
Methanol
O-C,H
O-V
V5+ 2p1/2
V4+ 2p1/2
V3+ 2p1/2
V5+ 2p3/2
V4+ 2p3/2
V3+ 2p3/2
Intensity (a.u.)
540 535 530 525 520 515 510
Binding energy (eV)
(b)
Methanol
After etching
V-C
Before etching
C-O
C-C
Intensity (a.u.)
290 285 280
Binding energy (eV)
(c)
Water
O-C,H
O-V
V5+ 2p1/2
V4+ 2p1/2
V5+ 2p3/2
V4+ 2p3/2
Intensity (a.u.)
540 535 530 525 520 515 510
Binding energy (eV)
(d)
Water
After etching
Before etching
C-O
C-C
Intensity (a.u.)
290 285 280
Binding energy (eV)

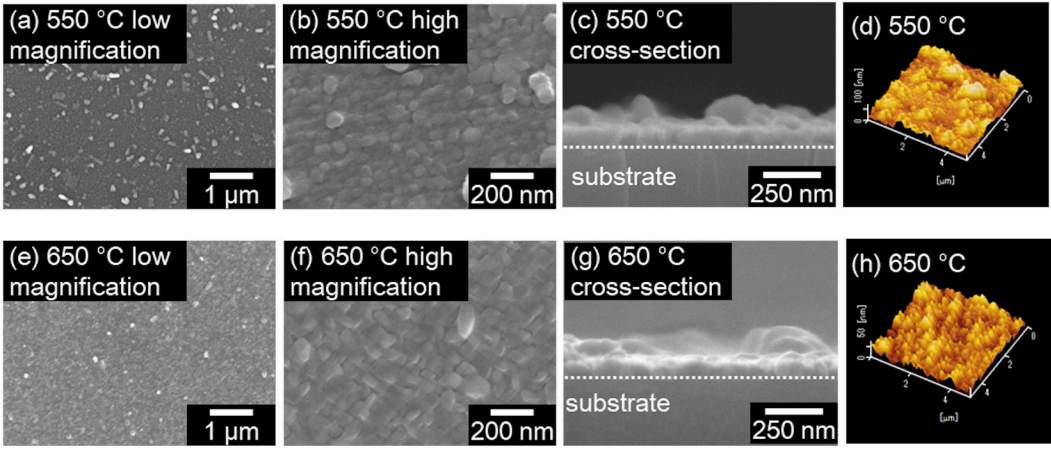
(a) 550 °C low magnification
1 µm
(b) 550 °C high magnification
200 nm
(c) 550 °C cross-section
substrate
250 nm
(d) 550 °C
100 [nm]
0
2
4
[µm]
(e) 650 °C low magnification
1 µm
(f) 650 °C high magnification
200 nm
(g) 650 °C cross-section
substrate
250 nm
(h) 650 °C
50 [nm]
0
2
4
[µm]

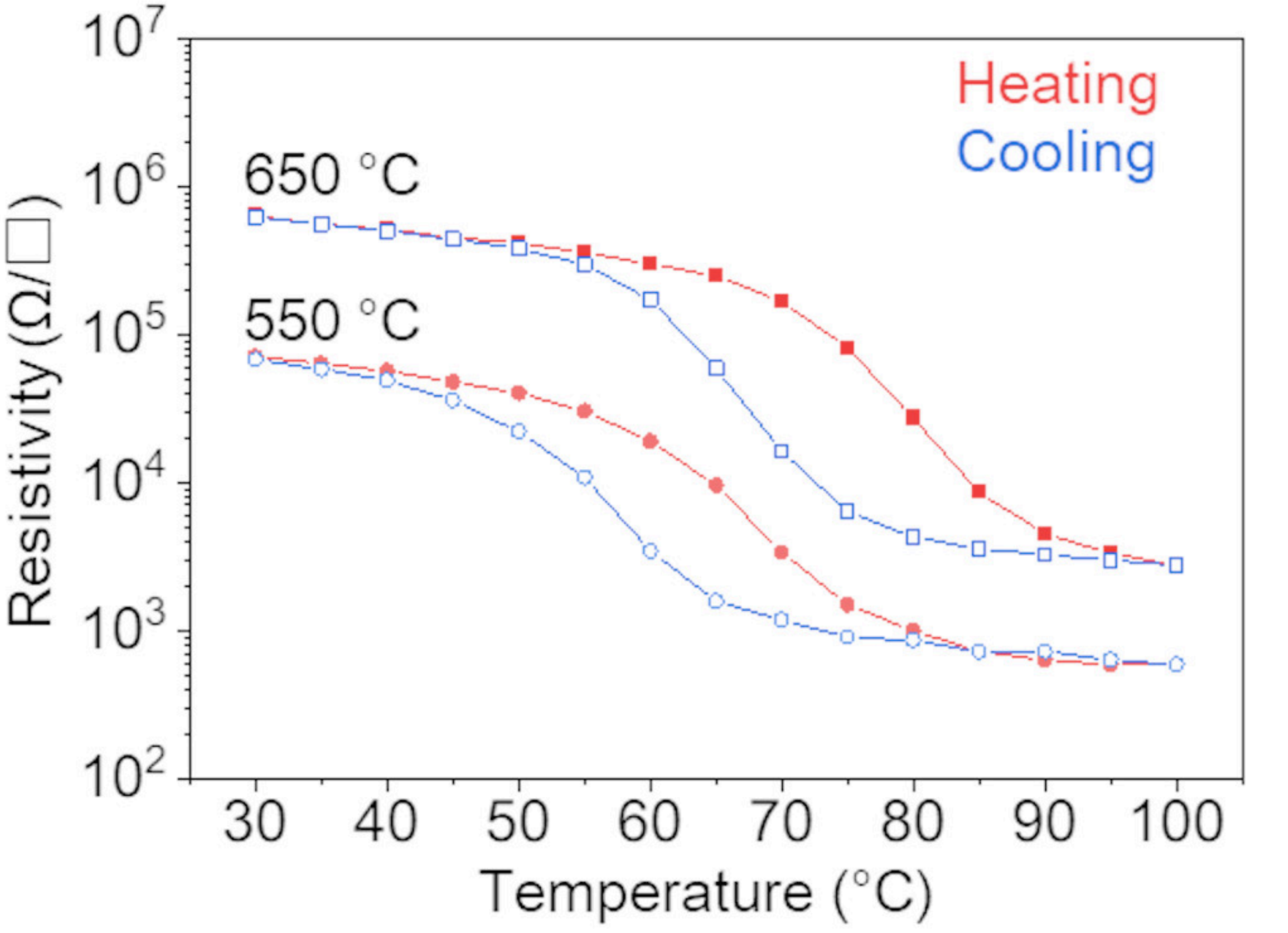
Heating
Cooling
650 °C
550 °C
Resistivity (Ω/□)
10^7
10^6
10^5
10^4
10^3
10^2
30
40
50
60
70
80
90
100
Temperature (°C)

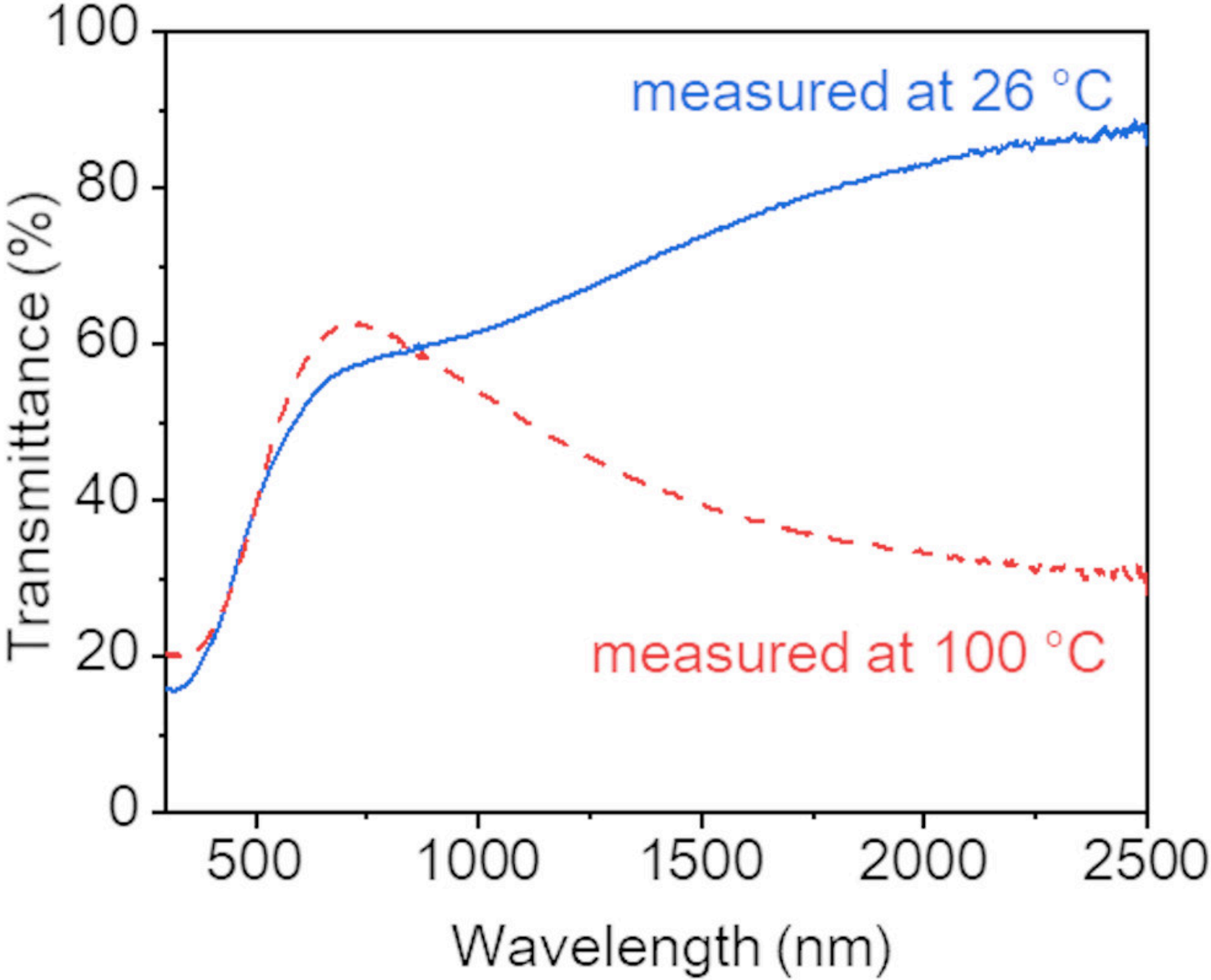
100
80
60
40
20
0
Transmittance (%)
500
1000
1500
2000
2500
Wavelength (nm)
measured at 26 °C
measured at 100 °C

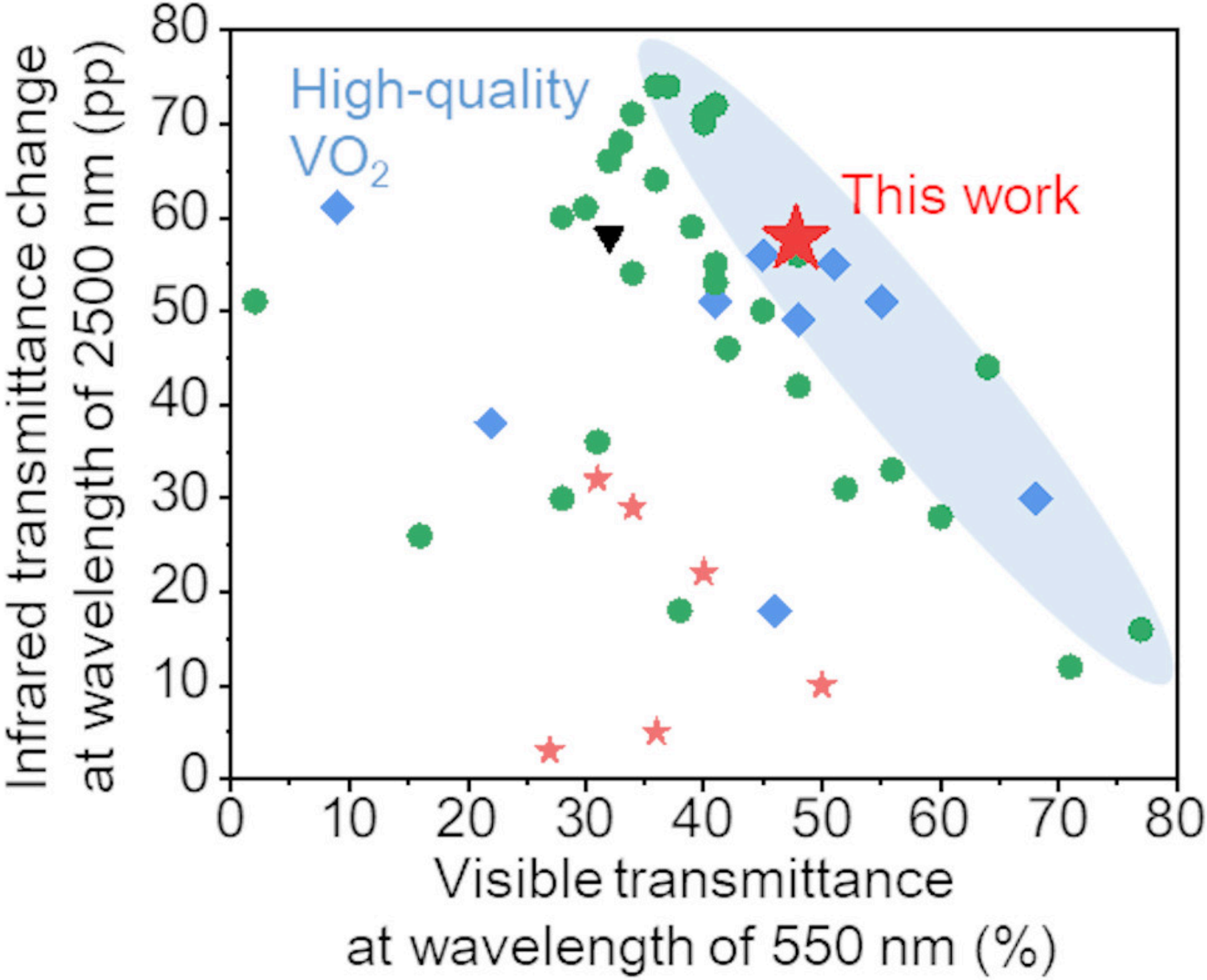
High-quality
VO2
This work
Infrared transmittance change
at wavelength of 2500 nm (pp)
Visible transmittance
at wavelength of 550 nm (%)
0
10
20
30
40
50
60
70
80